JGR Biogeosciences

RESEARCH ARTICLE
10.1029/2025JG009485

Special Collection:
Ecological Forecasting in the Earth System

Effective Short-Term Forecasting Strategies to Improve LULC Projections in Threatened Ecosystems

Johny Arteaga[1] and **Hugo Fort**[2]

[1]United States Department of Agriculture UV-B Monitoring and Research Program, Natural Resource Ecology Laboratory, Colorado State University, Fort Collins, CO, USA, [2]Instituto de Física Universidad de la República, Montevideo, Uruguay

Key Points:

- Time-series forecasting methods, including a Lotka-Volterra inspired and ARIMA, effectively predict sets of five consecutive years over the Rio de la Plata Grasslands
- Our methodology provides a framework to evaluate the short-term temporal performance of LULC models using historical annual time series
- The growing availability of long-term annual LULC maps is essential for supporting short-term projections in threatened ecosystems

Correspondence to:
J. Arteaga,
johny.arteaga.guarumo@gmail.com

Citation:
Arteaga, J., & Fort, H. (2025). Effective short-term forecasting strategies to improve LULC projections in threatened ecosystems. *Journal of Geophysical Research: Biogeosciences*, *130*, e2025JG009485. https://doi.org/10.1029/2025JG009485

Received 9 OCT 2025
Accepted 24 NOV 2025

Author Contributions:
Conceptualization: Johny Arteaga, Hugo Fort
Formal analysis: Johny Arteaga, Hugo Fort
Investigation: Johny Arteaga, Hugo Fort
Methodology: Johny Arteaga, Hugo Fort
Validation: Johny Arteaga, Hugo Fort
Writing – review & editing: Johny Arteaga, Hugo Fort

Abstract Recent advancements in remote sensing imagery classification have greatly improved monitoring of land use/land cover (LULC) dynamics, deepening our understanding of their effects on ecosystems and terrestrial nutrient cycling. Forecasting LULC change remains challenging because it is strongly influenced by socioeconomic drivers and biogeochemical processes linked to land management and climate change. To address this complexity, a wide range of models has been developed, from process-based to statistical approaches. Yet, comparisons at regional and global scales reveal large discrepancies, underscoring the need for more consistent calibration and validation with historical observations. Here, we leverage the increasing availability of annual LULC maps to evaluate the temporal performance of two independent data-driven approaches: ARIMA time-series forecasting and a deterministic Lotka–Volterra ecological-inspired model, across the Río de la Plata Grasslands, a threatened South American ecosystem. Both methods outperformed memoryless Markov chain models in capturing annual LULC transitions without requiring time-consuming processing spatial inputs. These results demonstrate that incorporating long-term annual LULC histories can substantially improve predictive skill and provide a robust framework for model intercomparison, with clear implications for linking land-cover change to ecosystem and Earth system modeling.

Plain Language Summary Researchers examined how to better predict changes in land use and land cover (LULC), for example, the shifts between crops, grasslands, and forests. We tested two different forecasting methods: ARIMA, a statistical time-series model, and a Lotka-Volterra-inspired ecological model, in the Río de la Plata Grasslands of South America. Both methods used long-term annual land-cover data and performed better than traditional Markov chain models, which do not account for past trends. The results show that using detailed historical LULC data can make short-term predictions more accurate and help improve comparisons among different LULC models, ultimately strengthening links between land-cover change and ecosystem modeling.

1. Introduction

Land Use and Land Cover Change (LULCC) reflects the human-driven transformation of natural landscapes through agricultural expansion, urbanization, afforestation, and climate change. These processes can cause the encroachment of woody vegetation into grasslands, the loss of coastal wetlands, and widespread deforestation in tropical regions (Sleeter et al., 2018). LULCC is a major driver of global environmental change, contributing to biodiversity loss (Díaz et al., 2019) and altering watershed dynamics (Haddeland et al., 2014). It has also reshaped the carbon balance of terrestrial ecosystems by reducing their capacity to sequester atmospheric carbon dioxide (CO_2) in soils and vegetation. Land conversions, particularly from forests to croplands, have accelerated biomass turnover, accounting for about 30% of total anthropogenic CO_2 emissions (Erb et al., 2016) and making LULCC the second-largest source of human-induced CO_2 release to the atmosphere (Friedlingstein et al., 2024). Beyond the carbon cycle, agricultural intensification has profoundly altered terrestrial nitrogen dynamics, with fertilizer use on N-fixing crops substantially increasing emissions of reactive nitrogen species (NO_x, NH_3) in recent decades (Tian et al., 2020).

Modeling spatiotemporal LULC transformations requires accounting for interactions among climate conditions, socioeconomic drivers, and landscape attributes. This complexity has traditionally been addressed using rule-based approaches such as cellular automata (CA) and agent-based models (Clarke, 2021). In CA-based models, temporal dynamics are often represented either by linearly extrapolating historical LULC trends (Hewitt & Diaz-Pacheco, 2017) or by applying memoryless processes, such as Markov chains (Liang et al., 2021),

which typically operate with decadal time steps. More recently, deep learning methods have been introduced to improve short-term spatiotemporal predictions (Cao et al., 2019). For example, long short-term memory (LSTM) models have been used to capture temporal dependencies and project greenhouse gas emissions associated with future LULCC, based on land-use transitions observed between 1992 and 2020 (Li et al., 2024). In parallel, a family of process-based models explicitly represents the socioeconomic dimensions of LULC, including the influence of economic dynamics on agricultural expansion (Sands et al., 2014; Van Asselen & Verburg, 2013).

Intercomparison studies of LULC models at regional and global scales have shown considerable variability in temporal predictions (Bayer et al., 2021), underscoring the need to evaluate models against historical data, despite uncertainties that can affect calibration, training, and predictive skill (Alexander et al., 2017). Such evaluation depends critically on the availability of consistent, high-quality LULC data sets.

Historically, LULCC has been studied using LULC maps generated through visual interpretation of aerial imagery or terrestrial surveys. Today, these methods have evolved into semi-automated classification techniques using satellite imagery and machine learning. Satellite data has greatly improved the quality of LULC maps through consistent spatiotemporal coverage, frequent revisit times, and moderate to high spatial resolution, exemplified by publicly available data sets such as Landsat and MODIS. Despite certain limitations (Ban et al., 2015), these products have enabled coordinated efforts at regional and global scales to produce long-term annual LULC maps (Parente et al., 2024; USGS, 2024) and track near real-time changes (Brown et al., 2022). From our perspective, these developments provide a valuable opportunity to strengthen short-term (<10 years) LULCC projections, particularly in regions undergoing rapid transformations.

In this work, we test whether time-series-based models can improve short-term LULC forecasts when trained on historical annual observations and systematically evaluated against withheld years. We compare two fundamentally different approaches: the temporal interaction generalized Lotka–Volterra (TIGLV) model, rooted in population ecology and entropy theory (Fort & Grigera, 2021), and the autoregressive integrated moving average (ARIMA) family of models, widely used in other disciplines but, to our knowledge, not yet applied to LULC forecasting (Hyndman & Athanasopoulos, 2021). Both are evaluated against traditional Markov chains across multiple spatial scales in the Río de la Plata Grasslands (RPG), using annual historical maps from the MapBiomas Trinational Pampa project. By integrating these methods with annual LULC data sets, this work provides a framework to support model intercomparison efforts and to enhance the reliability of short-term projections in dynamic landscapes.

2. Materials and Methods

2.1. Study Region

The RPG biome extends over central-east Argentina, south Brazil, and Uruguay in south America and is mainly occupied by native grassland threatened by croplands and exotic forest plantations (Baldi & Paruelo, 2008; Modernel et al., 2016). Four regions with different sizes were selected (Figure 1): the whole RPG biome, the Uruguayan territory, and two regions belonging to Uruguay identified with names C-24 and H-9, each one covering around 6.6×10^4 ha, where grassland has been significantly reduced by croplands and forest plantations, respectively (Brazeiro et al., 2020).

2.2. Land Use Land Cover Data Set

The Mapbiomas Pampa project generates annual maps of the Rio de la Plata grasslands, discriminating the following categories: native woody formation, forest plantation, wetlands, grasslands, agriculture, non-vegetated area, water, and non-observed. These maps are generated based on supervised machine-learning techniques of Landsat imagery (Baeza et al., 2022). The last collection, 3.0, represents improvements compared to previous collections providing LULC maps from 1985 to 2022 and quantified classification errors (Project MapBiomas Trinational Pampa, 2024). Time series and spatial distribution from collection 1.0 were accessed for regions C-24 and H-9 to evaluate the performance of the new forecasting methods compared to a previous study (Arteaga et al., 2024). The time series from collection 3.0 was used for Uruguay and the whole biome during the period 2000–2019.

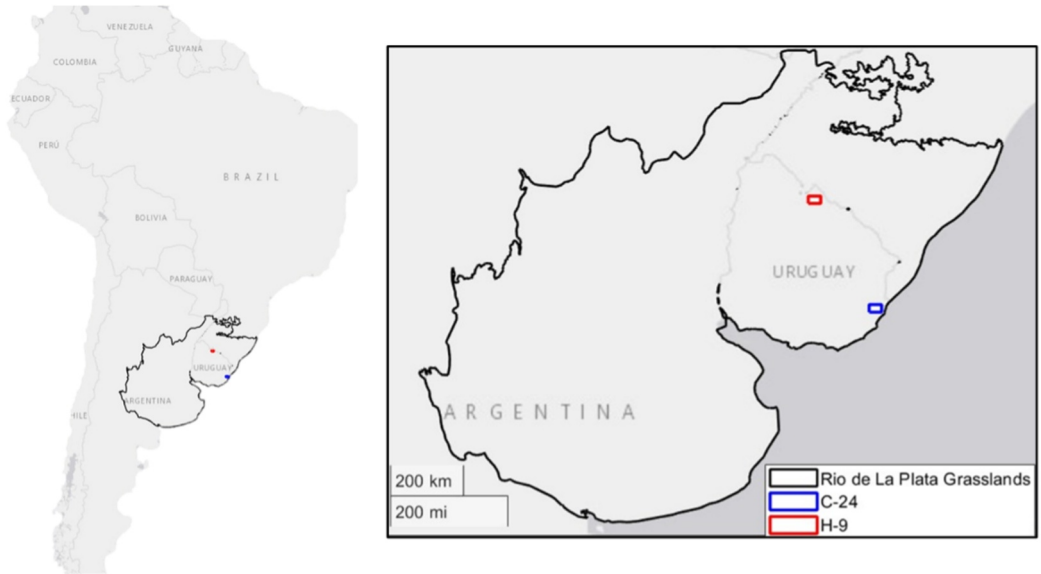

Figure 1. The Rio de la Plata Grasslands in South America. Regions C-24 and H-9 in Uruguay were identified with high anthropogenic pressure on native grasslands (Brazeiro et al., 2020).

2.3. Forecasting Methods

Across the four selected regions, we explored six validation/training periods to evaluate the performance of 5-year LULC time-series predictions using three different models. The first method is based on Markov chains, which needs gridded spatial information to quantify the transition matrix on regions C-24 and H-9. The second and third are the TIGLV and ARIMA methods, respectively, using only time series information to forecast across all the regions.

2.3.1. Markov Chains

We used Markov chains in regions C-24 and H-9 as a benchmark to compare the performance of TIGLV and ARIMA methods. Different methodologies can be used to quantify the predictions, in our case, the best performance was obtained through the following methodology: (a) Each region was divided into 1,058 quadrats with a size of 6.24 ha each; (b) for each year the dominant class was computed at each quadrat; (c) then, the transition matrices were computed by counting the number of quadrats dominated by class i in the year t to those dominated by class j in the year $t + \Delta t$, as

$$p_{ij}(t, t+\Delta t) = \frac{\text{Count}\left[N_{i\to j}(t, t+\Delta t) \right]}{\text{Count}\left[N_i(t) \right]}$$

(d) Finally, the forecast area is computed by the product between the ratio of occupied area $x_i(t) \equiv A_i(t)/A_{\text{Total}}$ and the transpose of the transition matrix, $x_i(t + \Delta t) = p_{ij}^T(t, t + \Delta t)\, x_i(t)$.

2.3.2. TIGLV Method

TIGLV, inspired by population dynamics, employs the Principle of Maximum Entropy (MaxEnt) to infer competitive interactions among different LULC classes, represented by the inverse of the covariance matrix C. TIGLV uses previous time-series information on the total area covered by each LULC class to generate forecasts, so the projected state at time $t + 1$ is approximated by the following equation:

$$A_i(t+1) = A_i(t) + r_i A_i(t)\left(1 + \sum_j \frac{\alpha_{ij} A_j(t)}{K_i}\right), \quad \forall \;\; i = 1, 2, \ldots, S \tag{1}$$

Here, $A_i(t)$ represents the area occupied by the i-LULC type, r_i is the intrinsic growth rate, and K_i is the carrying capacity. The matrix elements α_{ij}, belonging to the interaction matrix, are quantified during a given training time, T_t, by normalizing the inverse of the negative temporal covariance matrix C, with elements $C_{ij} = E\left[\left(A_i - \mu_i\right)\left(A_j - \mu_j\right)\right]$ that results from the pairwise covariances between the annual series of the LULC i and j within a training period, for example, $\alpha_{ij} = -C_{ij}^{-1}/|C_{ii}|$. Parameters r_i, and K_i are approximated by rearranging Equation 1 in a way that those parameters can be inferred from the coefficients of a linear regression built in the y-axis by the annual differences of $A_i(t)$ during the training period T_t, and in the x-axis by the product of the elements on the interaction matrix and $A_i(t)$ (see Equation 1 in Fort and Grigera (2021)). So, for a forecast period from 2011 to 2015, annual series of A_i are used from all preceding years up to and including 2010, to first compute α_{ij} and then perform the linear regression to estimate r_i, and K_i. This strategy represents an easy way to estimate this set of parameters, corresponding to a simplification that makes the analysis more tractable and can provide valuable insights. Still, it is crucial to recognize its limitations and has to be regarded as e effective quantities that do an excellent job of forecasting purposes (Emary & Fort, 2021). The algorithm to solve Equation 1 and obtain the associated parameters was implemented in a Jupyter Notebook in Python (see Data Availability Statement section).

2.3.3. ARIMA Models

This strategy was implemented at the LULC annual series for all four regions. ARIMA models are well-recognized statistical methods for predicting future behavior based on historical information. ARIMA models have three parameters to perform time-series forecast (p, d, q), where p is the time-series lag, d is the degree of differencing, and q is the moving average window. This model was implemented in MATLAB using the Econometric Toolbox; for a full model description, we suggest referring the reader to Hyndman and Athanasopoulos (2021).

To assess the best forecast based on the ARIMA models, we used the Akaike Information Criterion (AIC) and the Bayesian Information Criterion (BIC). We computed AIC and BIC scores for each model, selecting the one with the lowest AIC or BIC score as the best candidate for forecasting (Claeskins & Hkort, 2008). Specifically, we selected the model corresponding to the minimum score from either the AIC or BIC criterion for each training period. This comparison helps to identify not only which model fits the historical data best but also which one will likely perform better on unseen future data (James et al., 2014). Both criteria penalize adding parameters, thus helping to prevent overfitting, a common issue in time series modeling where a model fits noise rather than underlying patterns. AIC tends to favor more complex models when sample sizes are small (Akaike, 1974), while BIC provides a stronger penalty for additional parameters, making it more conservative (Schwarz, 1978).

2.4. Forecast Performance

Across the regions of interest, LULC time series were extracted from 2000 to 2019 by selecting the four dominant classes. A set of six 5-year short-term predictions was produced, beginning with the 2010–2014 interval and concluding with the 2015–2019 interval. The training period for each set of predictions extended from 2000 to the year preceding the initial forecast. For instance, the first forecast, utilized a training period spanning 2000–2009 to forecast the period 2010–2014, whereas in the final forecast used the expanded 2000–2014 period to forecast 2015–2019. The forecast performance for each method was evaluated by computing the forecast area for the LULC type i during the year t, $A_i(t)$, and its percentual relative error against the observed $A^{\text{obs}}{}_i(t)$. So, the Mean Absolute Percentual Error (MAPE) for each 5-year forecast is given by

$$\text{MAPE}_i(t) = \frac{1}{5}\sum_{t=T_t+1}^{T_t+6} \frac{\left|A_i(t) - A^{\text{obs}}{}_i(t)\right|}{A^{\text{obs}}{}_i(t)} \times 100 \tag{2}$$

This same metric was also used to evaluate the Markov chain's performance, but instead of using the area A we used the ratios x. The grand MAPE, defined as the average of the individual MAPEs for each forecast, was used to evaluate the overall short-term performance by averaging the MAPE over all 5 years.

To assess the uncertainty of each forecasting method across the different training sets and forecast horizons, we examined the error distribution (predicted − observed) and used the interquartile range (Q75 − Q25) as the

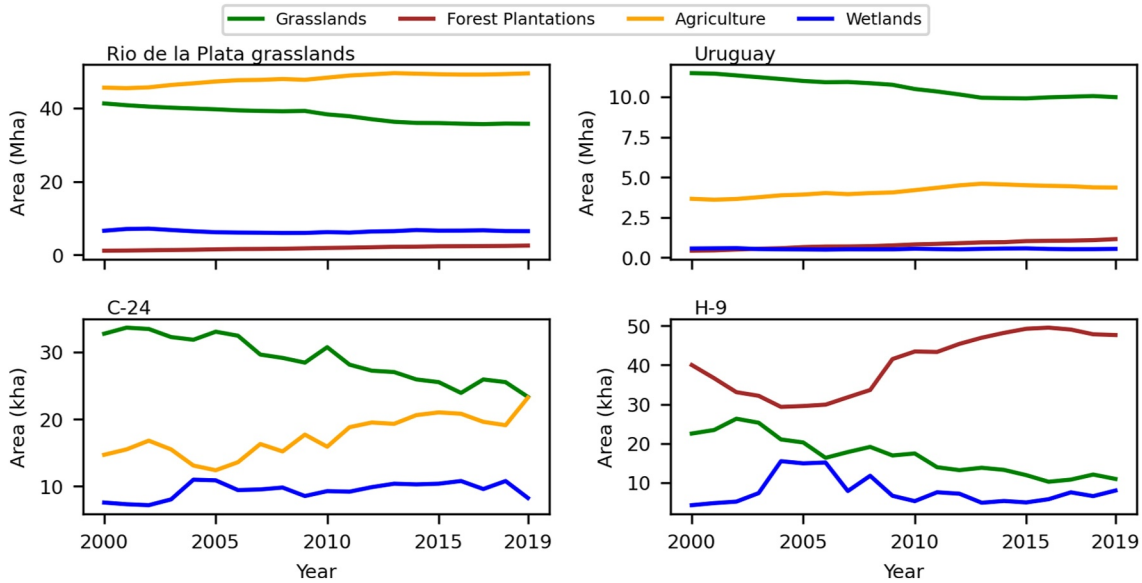

Figure 2. Annual LULCC from 2000 to 2019 for the most representative land-cover types at RPG, Uruguay, C-24, H-9.

uncertainty interval around the median error (Q50). This interval represents the variability in prediction errors for each LULC class across the five forecasted years and the full set of training periods.

3. Results

Figure 2 presents the four most representative LULC types retrieved by the Mapbiomas-Pampa project across all the regions. Grassland reduction is remarkable in all the regions, with a linear decay until 2012 in the whole biome and Uruguay. During this period, the entire RPG showed a dominance of crops, increasing their surface at the expense of grasslands. Forest plantations constantly increased throughout the study period, with a particularly higher trend in Uruguay. Despite the observed fluctuations, grassland reduction is evident in local regions, being replaced by Agriculture in C-24 and Forest Plantations in H-9.

The grand MAPE metric was used to assess overall performance across the complete set of 5-year forecast periods. TIGLV consistently performs well in regions C-24 and H-9 compared to the Markov approach, except during the training period 2000–2012, when Markov performed slightly better (Figure 3). Similarly, the best ARIMA model only obtains somewhat better performance than TIGLV during the training period 2000–2012 at region C-24 but outperforms the Markovian approach in most of the training periods, except for periods 2000–2009 and 2000–2012 at C-24 and 2000–2012 at H-9 (Figure 3). The grand MAPE boxplot distribution over all the training periods showed high performance of TIGLV at C-24 and H-9, followed by the best ARIMA and ending

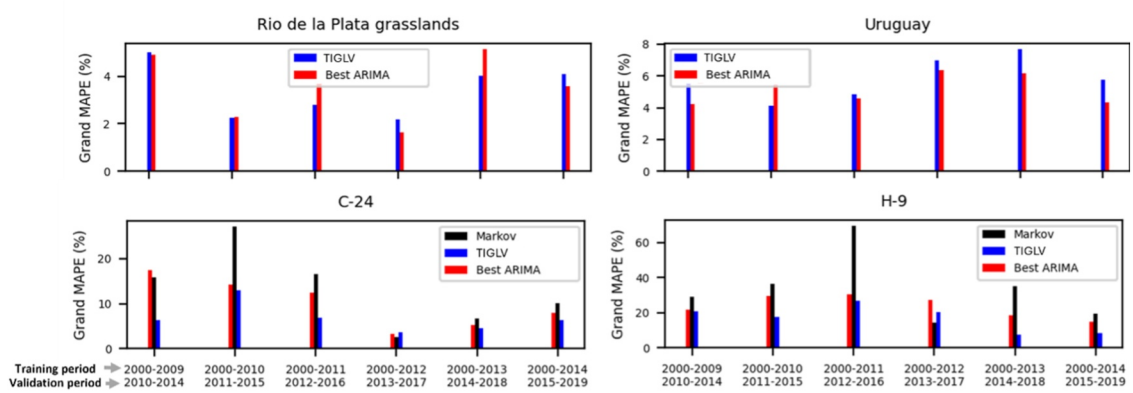

Figure 3. Grand MAPE (*y*-axis) obtained for each model (color) for the six different training/validation periods (*x*-axis) and the four regions of interest.

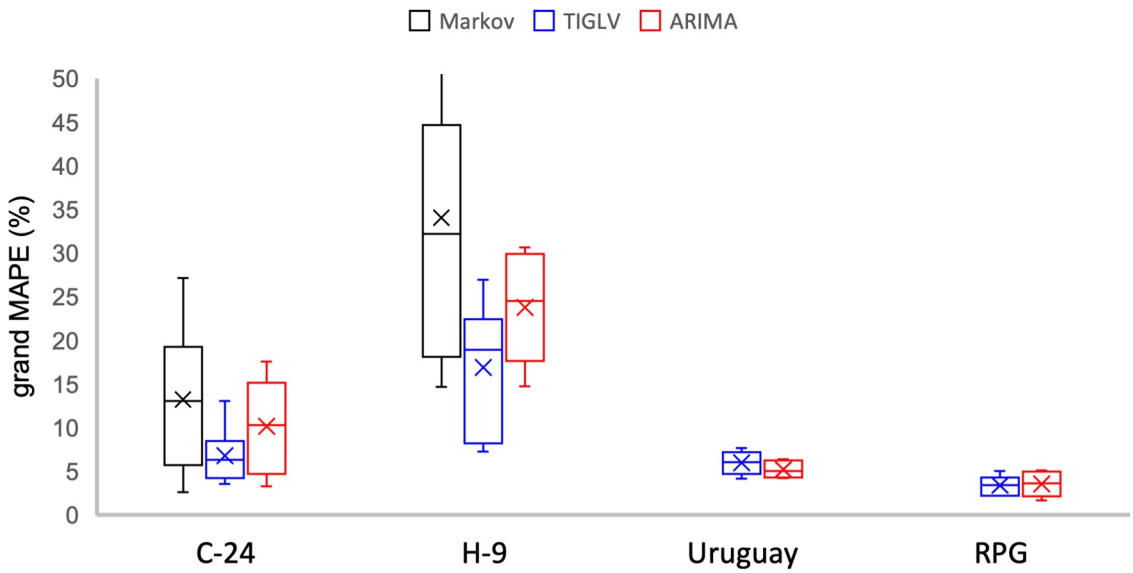

Figure 4. Boxplot of grand MAPE distributions obtained from each set of training/validation (Figure 3) for each model (color) across regions (*x*-axis). The cross symbol represents the mean grand MAPE across the full set.

with Markov (Figure 4). Regions H-9 showed the highest uncertainty, with average grand MAPE' ranging from 15% to 35% (Figure 4).

Without considering the Markov approach, the best ARIMA and TIGLV presented diverse performances depending on the training period and the region in Uruguay and the entire RPG. In Uruguay, the best ARIMA performed frequently better than TIGLV (Figure 3). The performance distribution over all training sets showed that the best ARIMA did a slightly better job in Uruguay, while TIGLV performed better in RPG (Figure 4). Additionally, a high forecast uncertainty was registered in small regions, whereas bigger regions presented lower uncertainty, staying below 5% in RPG (Figures 3 and 4).

Related to the best ARIMA method, the lowest error was obtained using the BIC information criterion at regions C-24 and H-9. Uruguay and the RPG showed similar performance regarding the AIC and BIC criteria (not shown). Additionally, the best results were obtained in combinations of p, d, and q parameters, taking values in the interval between [0,2].

The uncertainty interval for each forecast period tends to decrease as the training period length increases for regions C-24 and H-9, whereas for RPG and Uruguay the intervals remain similar (Figure 5). Moreover, we observed a consistent increase in uncertainty with longer forecast horizons (Figure 6).

4. Discussion

We studied the performance of three different approaches to forecasting short-term LULC temporal changes over a biome dominated by mesic grasslands in South America. We employed annual LULC maps provided by the Mapbiomas Pampa project, along the period 2000–2019 over two local regions in the northern (H-9) and east (C-24) of Uruguay. In these two regions, we confirmed the reduction of grasslands due to forest plantations in the north and cropland expansion in the east, consistent with previous findings (Brazeiro et al., 2020). Additionally, we observed substantial fluctuations in the land-cover time series, particularly in region H-9. For instance, the sudden and unexpected increase in wetland area between 2003 and 2007 (Figure 2) may be attributed to misclassification errors between map collections. This interpretation is supported by the more recent collection 3.0 product, in which the wetland extent remained nearly constant at values below 0.5 kha. Such inaccuracies, which tend to be amplified in smaller areas (Skakun, 2025), likely result from inherent uncertainties in remote sensing–based LULC classification. These include imperfections in training data, confusion among spectrally similar land-cover types over time and space, and inconsistencies in image quality due to factors such as cloud contamination. Consequently, these products typically exhibit overall regional accuracies of 75%–80%, with

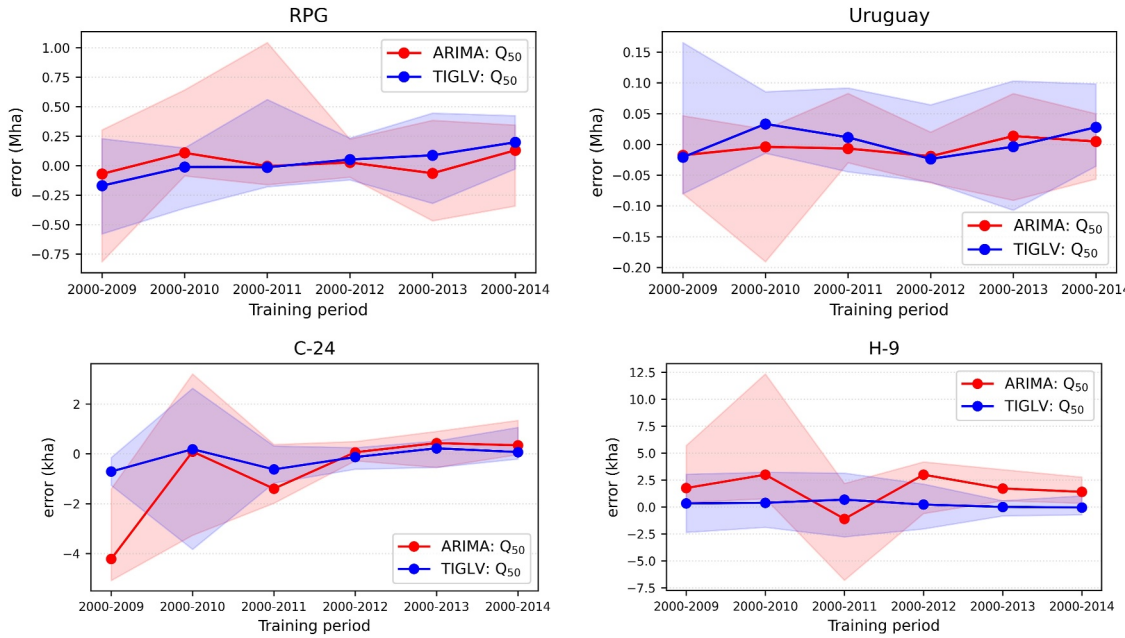

Figure 5. Interquartile range (shaded region) of ARIMA and TIGLV errors for each training period, shown around the median error (points).

wetlands, grasslands, and shrublands being among the most challenging classes to distinguish across platforms (Wang et al., 2023).

At regional scale, the entire RPG and Uruguayan territory, we observed the reduction of grasslands by Agriculture mainly during the period 2000–2012, corresponding to a period when commodity prices played an important role in increasing crops across the region (Pulp, paper, and allied products prices, n.d.). Forest Plantations constantly increased over the entire study period, with a higher rate in Uruguay, which might be associated with the expansion of Pinus plantations across the RPG (Dieguez et al., 2024). Wetlands, the third most dominant ecosystem, remained stable throughout the entire period.

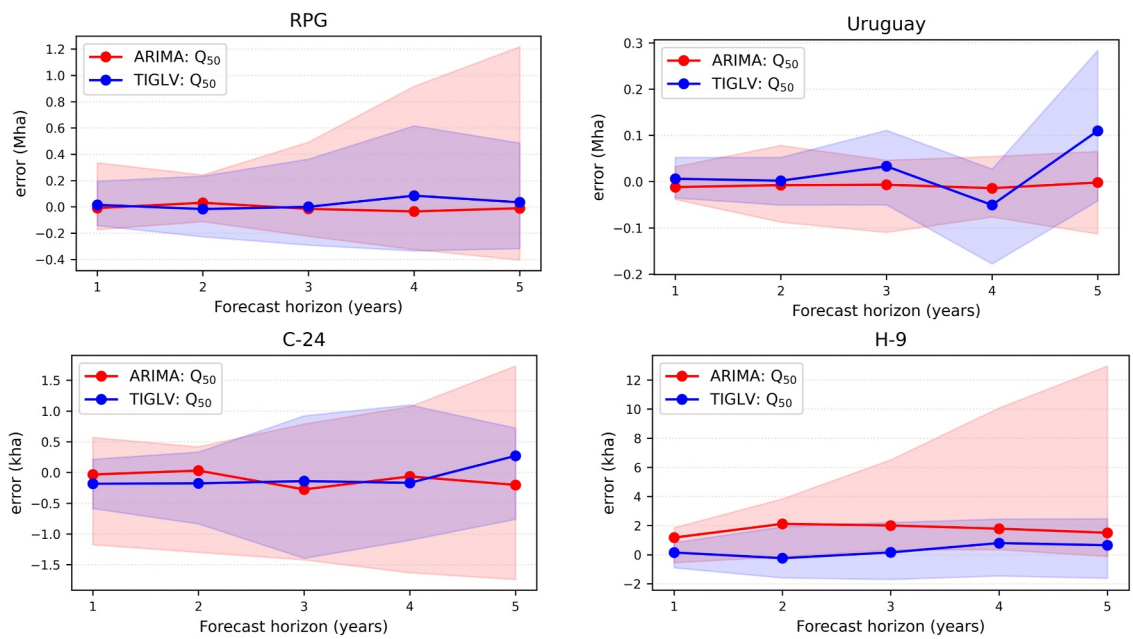

Figure 6. Interquartile range (shaded region) of ARIMA and TIGLV errors for each forecast horizon, shown around the median error (points).

The high fluctuations registered in regions C-24 and H-9 resulted in a good opportunity to test the robustness of the forecast methods when dealing with noisier time series. For instance, the high fluctuations registered in region H-9 showed the most significant errors among all the regions when even the best Markov approach, obtained after considering gridded spatial information, was outperformed by the best ARIMA and TIGLV. A less noisy region, C-24, with very steep trends, also shows a great average performance using TIGLV, obtaining half of the error registered by Markov (Figure 4). It is essential to mention that we kept collection 1.0 to analyze regions C-24 and H-9, despite its errors compared to collection 3.0, because it was a unique opportunity to compare with the performance of previously developed spatial methods like the spatial Lotka-Volterra and an alternative Markov strategy (Arteaga et al., 2024). The Markov strategy applied in this current work slightly outperformed the results of the hard-processing spatial strategies in this previous work.

At the regional scale, in the RPG and Uruguay, fluctuations were expected to have less impact on the total occupied areas, and both methods, ARIMA and TIGLV, presented similar performance, with errors around 5% and similar uncertainties within training periods. Overall, the two models based on only temporal information in projecting five consecutive years of LULC changes performed substantially better in regions with high LULC fluctuations than more demanding methods requiring spatial information processing. Notably, the TIGLV method performed better than ARIMA in areas with higher LULC changes, as observed in regions C-24 and H-9.

The uncertainty intervals for each forecast period show a clear decreasing trend in regions C-24 and H-9, likely due to the relatively constant interannual variability observed from 2014 to 2019 compared to the large fluctuations between 2000 and 2015 (Figure 5). Interestingly, during this high-fluctuation period, TIGLV exhibits a more symmetrical interquartile distribution around zero than ARIMA. In contrast, for Uruguay and RPG, the relationship of decreasing uncertainty with the increasing training-period length is much less clear (Figure 5). This may be because the 2000–2012 period showed a clear trend of sustained change, whereas both regions stabilized afterward (Figure 2). Given that prediction errors for these regions remain below 10% (Figure 4), the nearly invariant uncertainty intervals across training lengths likely reflect the inherent limits of forecasting when the target time series is almost constant. Overall, this analysis indicates that extending the training period does not necessarily reduce forecast uncertainty. Instead, a longer training history increases the diversity of training–validation configurations, enabling a more robust characterization of the uncertainty intervals.

The growth of forecast uncertainty with increasing prediction horizon is a fundamental property of time-series forecasting (Figure 6), often referred to as the uncertainty horizon (Christensen et al., 2018; Knüppel, 2018). This pattern emerges because uncertainty propagates and accumulates through the iterative forecasting process. Consequently, improving the accuracy of initial conditions is critical for LULC modeling, as doing so can reduce the compounding of uncertainty and improve the reliability of longer-term projections (Bayer et al., 2021; Prestele et al., 2016).

Advances in strategies to classify remote-sensing imagery to produce high-resolution annual LULC maps are fundamental to improving the science around the role of LULC transformations in natural ecosystems and supporting land management policies. These advances may significantly benefit spatiotemporal LULC modeling by exploiting short-term annual projections where historical trajectories may have a significant role (Cao et al., 2019).

An exciting challenge for these simple forecasting strategies is considering critical regions of LULC transitions, like those in drylands where grass-woodlands transitions are becoming more frequent (Ratajczak et al., 2017; Sala & Maestre, 2014). Detecting this area of vegetation shift would be ideal with a long temporal window, that is, two decades of annual LULC observations, to determine the limitations between different forecasting models (Lapeyrolerie & Boettiger, 2023).

5. Conclusions

We proposed two short-term forecasting strategies for LULC changes using two different time-series analysis methods, the TIGLV and ARIMA models. These methods outperformed more computationally expensive approaches based on spatial processing, such as Markov chains and previous Lotka–Volterra modeling, in regions C-24 and H-9. Both these regions exhibited higher temporal fluctuations than Uruguay and the RPG, while forecast performance gradually improved as the time series developed more defined trends. This strong performance across different spatial scales provides a proof of concept for incorporating temporal memory into

LULC modeling, as opposed to non-memory methods like Markov chains. Moreover, this initiative contributes to ongoing model intercomparison efforts by offering a framework to assess uncertainties among different families of LULC models through consistent short-term training and validation periods derived from annual LULC maps. In practice, improving the accuracy of short-term LULC forecasts can support rapid responses to deforestation and habitat loss, and enhance carbon-cycle modeling by providing timely estimates of land-cover transitions that drive changes in terrestrial carbon stocks and fluxes.

List of acronyms

AIC	Akaike Information Criterion
ARIMA	Autoregressive integrated moving averages
BIC	Bayesian Information Criterion
CA	Cellular Automata
LULC	Land Use and Land Cover
RPG	Río de la Plata Grasslands
TIGLV	Temporal Interaction Generalized Lotka-Volterra

Conflict of Interest

The authors declare no conflicts of interest relevant to this study.

Data Availability Statement

The data set and software used in this study are openly available in Arteaga and Fort (2025). *Data set*: The annual LULC time-series data (CSV format) for the four study regions are available in Arteaga and Fort (2025). *Software*: A Jupyter Notebook (IPYNB format) includes the Python subroutines used to implement the TIGLV method and compute the grand MAPE, with an example for region C-24. The notebook also contains a MATLAB script used to identify the optimal ARIMA model for each training/validation set, illustrating the calculations for the land-cover time series of Uruguay.

Acknowledgments
We acknowledge the editors and the reviewers for their great suggestions, which substantially improved the quality of this work.

References

Akaike, H. (1974). A new look at the statistical model identification. *IEEE Transactions on Automatic Control*, *19*(6), 716–723. https://doi.org/10.1109/tac.1974.1100705

Alexander, P., Prestele, R., Verburg, P. H., Arneth, A., Baranzelli, C., Batista e Silva, F., et al. (2017). Assessing uncertainties in land cover projections. *Global Change Biology*, *23*(2), 767–781. https://doi.org/10.1111/gcb.13447

Arteaga, J., Agudelo, J., Brazeiro, A., & Fort, H. (2024). A dynamical system to model land use interactions by using population dynamics: Application on vulnerable grasslands. *Proceedings of the Royal Society A: Mathematical, Physical and Engineering Sciences*, *480*(2301), 20240097. https://doi.org/10.1098/rspa.2024.0097

Arteaga, J., & Fort, H. (2025). TIGLV/ARIMA to predict LULC changes [Software & Dataset]. *Zenodo*. https://doi.org/10.5281/zenodo.17307466

Baeza, S., Vélez-Martin, E., De Abelleyra, D., Banchero, S., Gallego, F., Schirmbeck, J., et al. (2022). Two decades of land cover mapping in the Río de la Plata grassland region: The MapBiomas Pampa initiative. *Remote Sensing Applications: Society and Environment*, *28*, 100834. https://doi.org/10.1016/j.rsase.2022.100834

Baldi, G., & Paruelo, J. M. (2008). Land-use and land cover dynamics in South American temperate grasslands. *Ecology and Society*, *13*(2), art6. https://doi.org/10.5751/es-02481-130206

Ban, Y., Gong, P., & Giri, C. (2015). Global land cover mapping using Earth observation satellite data: Recent progresses and challenges. *ISPRS Journal of Photogrammetry and Remote Sensing*, *103*, 1–6. https://doi.org/10.1016/j.isprsjprs.2015.01.001

Bayer, A. D., Fuchs, R., Mey, R., Krause, A., Verburg, P. H., Anthoni, P., & Arneth, A. (2021). Diverging land-use projections cause large variability in their impacts on ecosystems and related indicators for ecosystem services. *Earth System Dynamics*, *12*(1), 327–351. https://doi.org/10.5194/esd-12-327-2021

Brazeiro, A., Achkar, M., Toranza, C., & Bartesaghi, L. (2020). Agricultural expansion in Uruguayan grasslands and priority areas for vertebrate and woody plant conservation. *Ecology and Society*, *25*(1), art15. https://doi.org/10.5751/es-11360-250115

Brown, C. F., Brumby, S. P., Guzder-Williams, B., Birch, T., Hyde, S. B., Mazzariello, J., et al. (2022). Dynamic world, near real-time global 10 m land use land cover mapping. *Scientific Data*, *9*(1), 251. https://doi.org/10.1038/s41597-022-01307-4

Cao, C., Dragićević, S., & Li, S. (2019). Short-term forecasting of land use change using recurrent neural network models. *Sustainability*, *11*(19), 5376. https://doi.org/10.3390/su11195376

Christensen, P., Gillingham, K., & Nordhaus, W. (2018). Uncertainty in forecasts of long-run economic growth. *Proceedings of the National Academy of Sciences*, *115*(21), 5409–5414. https://doi.org/10.1073/pnas.1713628115

Claeskins, G., & Hkort, N. (2008). *Model selection and model averaging (Cambridge Series in Statistical and Probabilistic Mathematics)* (1st ed.). Cambridge University Press.

Clarke, K. C. (2021). Cellular automata and agent-based models. In *Handbook of regional science* (pp. 1751–1766). Springer Berlin Heidelberg. Berlin, Heidelberg.

Díaz, S., Settele, J., Brondízio, E. S., Ngo, H. T., Agard, J., Arneth, A., et al. (2019). Pervasive human-driven decline of life on Earth points to the need for transformative change. *Science*, *366*(6471), eaax3100. https://doi.org/10.1126/science.aax3100

Dieguez, H., Piñeiro, G., & Paruelo, J. (2024). Unraveling impacts on carbon, water and energy exchange of Pinus plantations in South American temperate ecosystems. *Science of the Total Environment*, *953*, 176150. https://doi.org/10.1016/j.scitotenv.2024.176150

Emary, C., & Fort, H. (2021). Markets as ecological networks: Inferring interactions and identifying communities. *Journal of Complex Networks*, *9*(2), cnab022. https://doi.org/10.1093/comnet/cnab022

Erb, K. H., Fetzel, T., Plutzar, C., Kastner, T., Lauk, C., Mayer, A., et al. (2016). Biomass turnover time in terrestrial ecosystems halved by land use. *Nature Geoscience*, *9*(9), 674–678. https://doi.org/10.1038/ngeo2782

Fort, H., & Grigera, T. S. (2021). A method for predicting species trajectories tested with trees in Barro Colorado tropical forest. *Ecological Modelling*, *446*, 109504. https://doi.org/10.1016/j.ecolmodel.2021.109504

Friedlingstein, P., O'sullivan, M., Jones, M. W., Andrew, R. M., Hauck, J., Landschützer, P., et al. (2024). Global carbon budget 2024. *Earth System Science Data Discussions*, *2024*, 1–133.

Haddeland, I., Heinke, J., Biemans, H., Eisner, S., Flörke, M., Hanasaki, N., et al. (2014). Global water resources affected by human interventions and climate change. *Proceedings of the National Academy of Sciences*, *111*(9), 3251–3256. https://doi.org/10.1073/pnas.1222475110

Hewitt, R., & Diaz-Pacheco, J. (2017). Stable models for metastable systems? Lessons from sensitivity analysis of a Cellular Automata urban land use model. *Computers, Environment and Urban Systems*, *62*, 113–124. https://doi.org/10.1016/j.compenvurbsys.2016.10.011

Hyndman, R. J., & Athanasopoulos, G. (2021). Forecasting: Principles and practice (3rd ed.). OTexts: Melbourne, Australia. OTexts.com/fpp3.

James, G., Witten, D., Hastie, T., & Tibshirani, R. (2014). *An introduction to statistical learning: With applications in R*. Springer.

Knüppel, M. (2018). Forecast-error-based estimation of forecast uncertainty when the horizon is increased. *International Journal of Forecasting*, *34*(1), 105–116. https://doi.org/10.1016/j.ijforecast.2017.08.006

Lapeyrolerie, M., & Boettiger, C. (2023). Limits to ecological forecasting: Estimating uncertainty for critical transitions with deep learning. *Methods in Ecology and Evolution*, *14*(3), 785–798. https://doi.org/10.1111/2041-210x.14013

Li, L., Awada, T., Zhang, Y., & Paustian, K. (2024). Global land use change and its impact on greenhouse gas emissions. *Global Change Biology*, *30*(12), e17604. https://doi.org/10.1111/gcb.17604

Liang, X., Guan, Q., Clarke, K. C., Liu, S., Wang, B., & Yao, Y. (2021). Understanding the drivers of sustainable land expansion using a patch-generating land use simulation (PLUS) model: A case study in Wuhan, China. *Computers, Environment and Urban Systems*, *85*, 101569. https://doi.org/10.1016/j.compenvurbsys.2020.101569

Modernel, P., Rossing, W. A., Corbeels, M., Dogliotti, S., Picasso, V., & Tittonell, P. (2016). Land use change and ecosystem service provision in Pampas and Campos grasslands of southern South America. *Environmental Research Letters*, *11*(11), 113002. https://doi.org/10.1088/1748-9326/11/11/113002

Parente, L., Sloat, L., Mesquita, V., Consoli, D., Stanimirova, R., Hengl, T., et al. (2024). Annual 30-m maps of global grassland class and extent (2000–2022) based on spatiotemporal Machine Learning. *Scientific Data*, *11*(1), 1–22. https://doi.org/10.1038/s41597-024-04139-6

Prestele, R., Alexander, P., Rounsevell, M. D., Arneth, A., Calvin, K., Doelman, J., et al. (2016). Hotspots of uncertainty in land-use and land-cover change projections: A global-scale model comparison. *Global Change Biology*, *22*(12), 3967–3983. https://doi.org/10.1111/gcb.13337

Project MapBiomas Trinational Pampa. (2024). Collection [1.0 and 3.0] of the Annual Land Cover and Land Use Maps in Trinational Pampa. Retrieved from https://pampa.mapbiomas.org/

Pulp, paper, and allied products prices. (n.d.). Retrieved from https://fred.stlouisfed.org/series/WPU0911

Ratajczak, Z., D'Odorico, P., Nippert, J. B., Collins, S. L., Brunsell, N. A., & Ravi, S. (2017). Changes in spatial variance during a grassland to Shrubland state transition. *Journal of Ecology*, *105*(3), 750–760. https://doi.org/10.1111/1365-2745.12696

Sala, O. E., & Maestre, F. T. (2014). Grass–woodland transitions: Determinants and consequences for ecosystem functioning and provisioning of services. *Journal of Ecology*, *102*(6), 1357–1362. https://doi.org/10.1111/1365-2745.12326

Sands, R., Jones, C., & Marshall, E. P. (2014). Global drivers of agricultural demand and supply.

Schwarz, G. (1978). Estimating the dimension of a model. *Annals of Statistics*, *6*(2), 461–464. https://doi.org/10.1214/aos/1176344136

Skakun, S. (2025). The impact of map accuracy on area estimation with remotely sensed data within the stratified random sampling design. *Remote Sensing of Environment*, *326*, 114805. https://doi.org/10.1016/j.rse.2025.114805

Sleeter, B. M., Liu, J., Daniel, C., Rayfield, B., Sherba, J., Hawbaker, T. J., et al. (2018). Effects of contemporary land-use and land-cover change on the carbon balance of terrestrial ecosystems in the United States. *Environmental Research Letters*, *13*(4), 045006. https://doi.org/10.1088/1748-9326/aab540

Tian, H., Xu, R., Canadell, J. G., Thompson, R. L., Winiwarter, W., Suntharalingam, P., et al. (2020). A comprehensive quantification of global nitrous oxide sources and sinks. *Nature*, *586*(7828), 248–256. https://doi.org/10.1038/s41586-020-2780-0

U.S. Geological Survey (USGS). (2024). *Annual NLCD collection 1 science products*. U.S. Geological Survey Data Release. https://doi.org/10.5066/P94UXNTS

Van Asselen, S., & Verburg, P. H. (2013). Land cover change or land-use intensification: Simulating land system change with a global-scale land change model. *Global Change Biology*, *19*(12), 3648–3667. https://doi.org/10.1111/gcb.12331

Wang, Y., Sun, Y., Cao, X., Wang, Y., Zhang, W., & Cheng, X. (2023). A review of regional and global scale land use/land cover (LULC) mapping products generated from satellite remote sensing. *ISPRS Journal of Photogrammetry and Remote Sensing*, *206*, 311–334. https://doi.org/10.1016/j.isprsjprs.2023.11.014